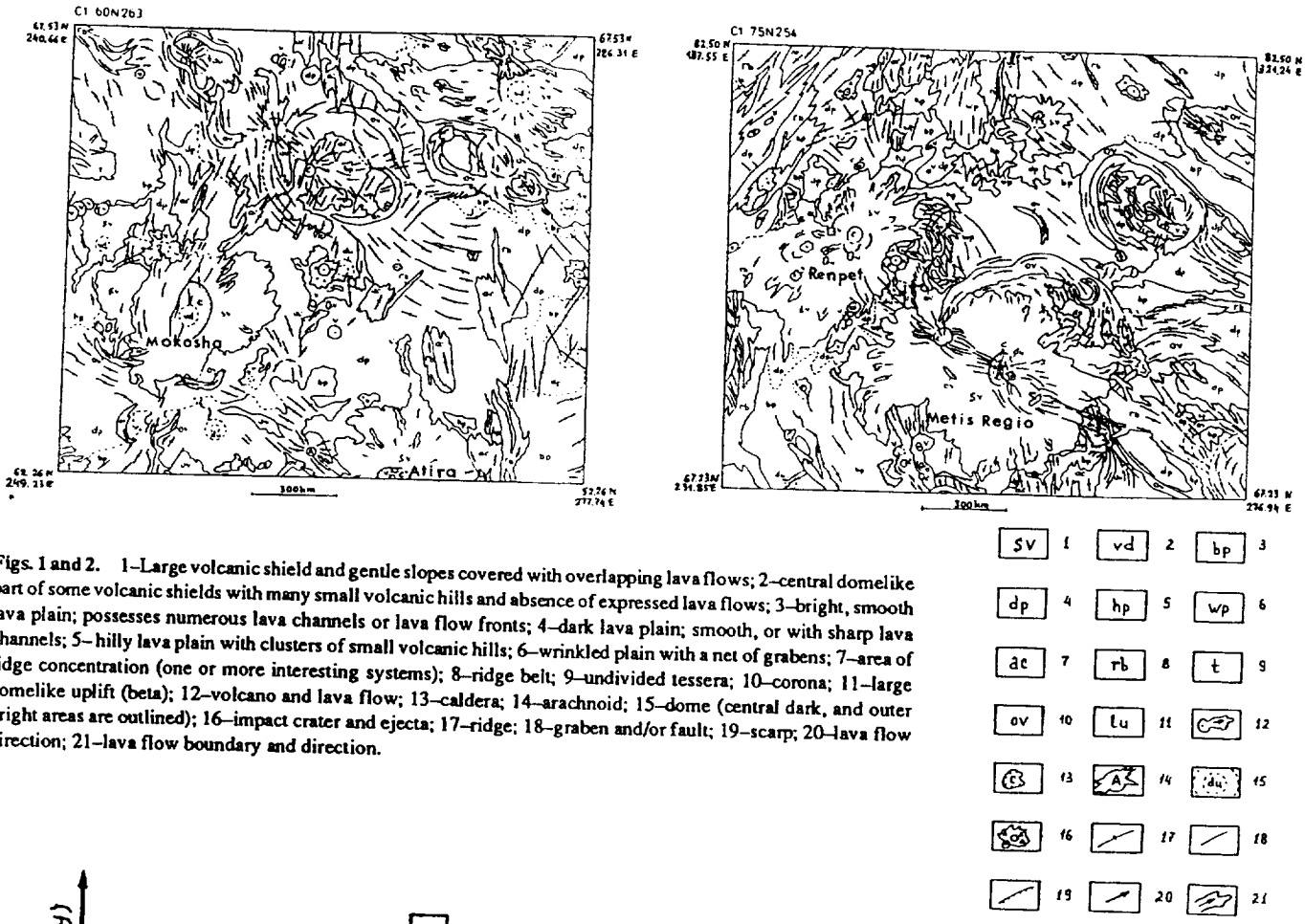

Figs. 1 and 2. 1–Large volcanic shield and gentle slopes covered with overlapping lava flows; 2–central domelike part of some volcanic shields with many small volcanic hills and absence of expressed lava flows; 3–bright, smooth lava plain; possesses numerous lava channels or lava flow fronts; 4–dark lava plain; smooth, or with sharp lava channels; 5–hilly lava plain with clusters of small volcanic hills; 6–wrinkled plain with a net of grabens; 7–area of ridge concentration (one or more interesting systems); 8–ridge belt; 9–undivided tessera; 10–corona; 11–large domelike uplift (beta); 12–volcano and lava flow; 13–caldera; 14–arachnoid; 15–dome (central dark, and outer bright areas are outlined); 16–impact crater and ejecta; 17–ridge; 18–graben and/or fault; 19–scarp; 20–lava flow direction; 21–lava flow boundary and direction.

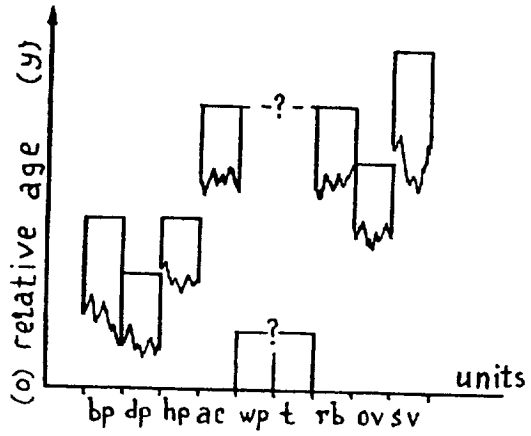

Fig. 3. Correlation of the mapped units shown in Figs. 1 and 2.

of Venus, 1:15,000,000 topographic series, northern hemisphere, V. 15M 90/G. I–2059. U.S. Geol. Surv.

N93-14376 484377

GEOID, TOPOGRAPHY, AND CONVECTION-DRIVEN CRUSTAL DEFORMATION ON VENUS.

Mark Simons, Bradford H. Hager, and Sean C. Solomon, Department of Earth, Atmospheric, and Planetary Sciences, Massachusetts Institute of Technology, Cambridge MA 02139, USA.

Introduction: High-resolution Magellan images and altimetry of Venus reveal a wide range of styles and scales of surface deformation [1] that cannot readily be explained within the classical terrestrial plate tectonic paradigm. The high correlation of long-wavelength topography and gravity and the large apparent depths of compensation suggest that Venus lacks an upper-mantle low-viscosity zone [2–5]. A key difference between Earth and Venus may be the degree of coupling between the convecting mantle and the overlying lithosphere. Mantle flow should then have recognizable signatures in the relationships between surface topography, crustal deformation, and the observed gravity field [6,7].

Model: We explore the effects of this coupling by means of a finite element modeling technique. The crust and mantle in these models are treated as viscous fluids. We solve both the equations of motion and the heat equation at every time step using a modified version of the two-dimensional Cartesian finite-element program ConMan [8]. A passive marker chain tracks the crust-mantle interface and permits variation in the crustal buoyancy as well as specific crustal and mantle rheologies. These rheologies depend on composition, temperature, and stress. In addition to the flow field, the stress field in the lithosphere, the surface topography, and the resulting geoid are readily calculated. The models presented here use an irregular finite-element mesh that is 50 elements high and 160 elements wide. Our maximum resolution is in the 40-km-thick top layer, where each element is 2 km high and 5 km wide. In all, the mesh is 800 km in the horizontal dimension and 400 km in the vertical dimension. We impose free-slip boundary conditions on the top and side walls, with no flow through these walls. Flow at the bottom boundary is constrained to be vertical with no horizontal flow permitted. This last boundary condition gives a virtual 800 km × 800 km box. The surface topography is calculated from the vertical stresses on the top wall of the box. Top and bottom

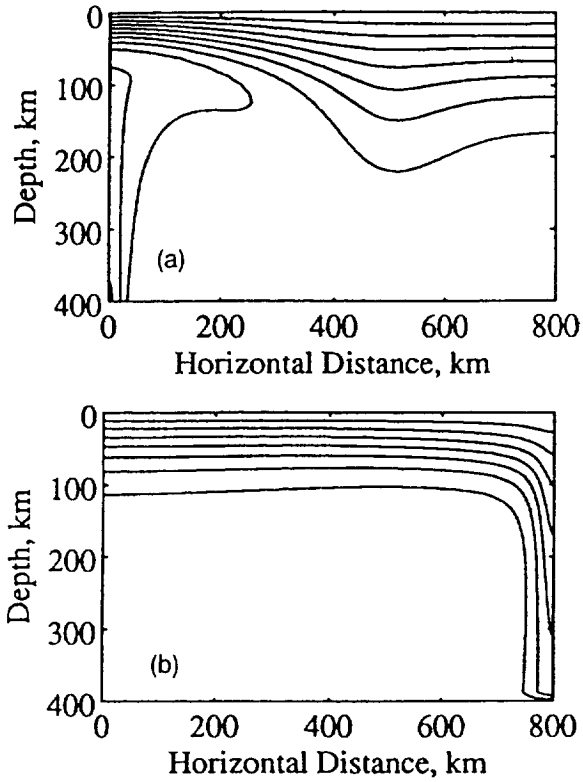

Fig. 1. Temperature contours at 130 m.y. for the (a) upwelling and (b) downwelling models. Contour interval is 100°C; the top of the box is at 500°C.

temperatures are fixed at 500°C and 1250°C respectively. Initially, we impose a linear temperature gradient across the lithosphere and set the rest of the mantle to be isothermal. We investigate two classes of models. Flow in the first class is initiated with a sinusoidal temperature perturbation throughout the box. This results in mantle flow that is dominated by concentrated downwelling (Fig. 1b). In the second class of models, flow is driven by a hot patch at the side of the box, thereby driving flow by concentrated upwelling (Fig. 1a).

Results: In all our models, convection produces horizontal compressional stresses in lithosphere above downwelling mantle and extensional stresses in lithosphere above upwelling mantle. As the convective vigor increases so does the magnitude of the stress. In models with constant-viscosity mantle overlain by a constant-viscosity crust, stress in the crust reaches values in excess of 100 MPa in less than 100 m.y. We find that the rate of increase in compressive stress decreases with increasing crustal viscosity. This is because the stronger the crust, the more the development of the convective instability in the mantle driving the deformation is impeded. We also find that the magnitude of the peak compressive stress achieved above the downwelling increases with higher viscosities and/or with thinner initial crustal layers; the stronger the crustal lid, the more tractions from mantle convection are supported in the crust. Since force balance on the crust requires that shear traction integrated along the base be balanced by normal tractions integrated through its thickness, the thinner the crust, the larger the horizontal stresses.

Both analytical models [9,10] and our numerical models of convection-induced crustal flow indicate that the amplitude and sign of the topography are highly time and rheology dependent. In general, possible responses of the crust to mantle flow can be divided into three categories. The first involves little if any crustal flow, and topography results mainly from the transmission of normal tractions induced by density contrasts within the mantle. The second possible regime involves substantial crustal flow, with geologically rapid thickening over convective downwelling and thinning over convective upwelling. In this regime the effects of crustal thickness variations dominate the topography. A third possible regime lies between the first two, with "in phase" deformation on short timescales and crustal flow on longer timescales. A strong mantle lithosphere tends to shield the crust from convective shear tractions, and topography results mainly from the transmission of convective normal tractions. A relatively weak lower crust facilitates crustal deformation, and the isostatic effects of crustal thickness variations dominate the topography.

Consideration of geoid to topography ratios (GTRs) can restrict which regime of crustal response is appropriate for Venus. The distribution of estimated GTRs for several highland regions on Venus is bimodal with two clusters around 10 and 25 m/km [5]. The positive correlation of long-wavelength gravity and topography implies that there are no major regions that have negative GTRs. To keep the GTRs positive, the geoid must follow the surface topography in sign at all times. Although the regime of negligible crustal flow can correctly predict both the sign and magnitude of the GTRs, it does not allow for the crustal deformation (i.e., flow) inferred from observations of tectonic features on Venus.

In contrast to the regime of negligible flow, that of time-dependent crustal flow generates topography that changes sign. Over a mantle downwelling, the topography is negative in the early stages of deformation and positive in the later stages of deformation; the converse holds over a mantle upwelling. During the transitional period the topography goes through zero, the geoid does not go through zero, and the GTR is unbounded; this singularity is not observed on Venus. An example of the evolution of the GTR for a model in the time-dependent regime is shown in Fig. 2. Note that before 90 m.y. both topography and geoid are negative, but at 90 m.y. crustal thickening effects begin to dominate and the topography switches sign, causing the GTRs to first become unbounded and then negative.

In the absence of a mechanism by which the sign of the geoid anomaly mimics that of the topography over a given upwelling or downwelling, only the regime of rapid crustal flow is plausible. In the case of mantle downwelling this would also require that the

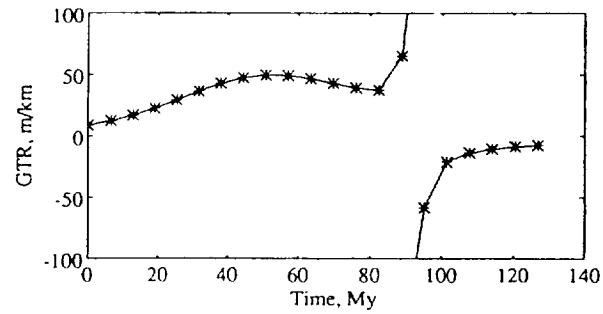

Fig. 2. Evolution of GTR with time. At each time step, the GTR shown is the slope of the best fit line to the collection of geoid and topography values upward continued to 250 km above the surface nodes in the model. The result is for a downwelling model, with a crust of constant viscosity 50 times that of the mantle. In this model the sign of the topography is time-dependent, but that of the geoid is not. The singularity at about 90 m.y. corresponds to the time when topography crosses the zero datum. Note that the GTRs for this model are neither always positive nor always bounded.

lower mantle be more viscous than the upper mantle in order to produce the required positive geoid anomalies. This has already been shown to be true for the Earth, where the observed geoid highs over regions of mantle upwelling and regions of mantle downwelling are best explained by the presence of a strong lower mantle [11,12]. The large positive GTRs and the presence of large shield volcanos in certain highland regions on Venus, such as Beta Regio and Eistla Regio, are best explained as areas of mantle upwelling [5,13,14]. The regime of rapid crustal flow predicts crustal thinning over the upwelling. However, the extensive partial melt and ensuing volcanism expected over such regions of mantle may outweigh the effects of crustal thinning on the surface topography and thus also yield postive GTRs [15].

References: [1] Solomon S. C. et al. (1991) *Science, 252*, 297. [2] Kiefer W. S. et al. (1986) *GRL, 13*, 14. [3] Bills B. G. et al. (1987) *JGR, 92*, 10. [4] Phillips R. J. et al. (1991) *Science, 252*, 651. [5] Smrekar S. E. and Phillips R. J. (1991) *EPSL, 107*, 587. [6] Phillips R. J. (1986) *GRL, 13*, 1141. [7] Phillips R. J. (1990) *JGR, 95*, 1301. [8] King S. D. et al. (1990) *PEPI, 59*, 195. [9] Bindschadler D. L. and Parmentier E. M. (1990) *JGR, 95*, 21. [10] Schmeling H. and Marquart G. (1990) *GRL, 17*, 2417. [11] Richards M. A. and Hager B. H. (1984) *JGR, 89*, 5987. [12] Hager B. H. (1984) *JGR, 89*, 6003. [13] Grimm R. E. and Phillips R. J. (1991) *JGR, 96*, 8305. [14] Grimm R. E. and Phillips R. J. (1991) *JGR*, in press. [15] Phillips R. J. et al. (1991) *Science, 252*, 651.

N93-14377

VENUS GRAVITY: SUMMARY AND COMING EVENTS.

W. L. Sjogren, Jet Propulsion Laboratory, 4800 Oak Grove Drive, Pasadena CA 91109, USA.

The first significant dataset to provide local measures of venusian gravity field variations was that acquired from the Pioneer Venus Orbiter (PVO) during the 1979–1981 period. These observations were S-band Doppler radio signals from the orbiting spacecraft received at Earth-based tracking stations. Early reductions of these data were performed using two quite different techniques. Estimates of the classical spherical harmonics were made to various degrees and orders up to 10 [1,2,3]. At that time, solutions of much higher degree and order were very difficult due to computer limitations. These reductions, because of low degree and order, revealed only the most prominent features with poor spatial resolution and very reduced peak amplitudes.

Another reduction technique was the line-of-sight acceleration mapping that had been used successfully for the Moon and Mars. This approach provided much more detail and revealed the high correlation of gravity with topography [4,5,6]. However, this technique does not produce a global field as do the spherical harmonics. It provided a mapping of features from approximately 50°N to 25°S latitude for 360° of longitude. Other shortcomings were that the accelerations were at spacecraft altitude rather than at the surface and were not vertical accelerations; however, the reductions were quick and cheaply accomplished. Other efforts to analyze these data included local area reductions, where surface masses were estimated [7,8,9].

The computer revolution over the past 10 years has allowed new reductions with spherical harmonics. New fields up to degree and order fifty (2600 parameters) have been made [10,11,12]. These fields now provide the best representation for any serious geophysicist doing quantitative modeling. There is now vertical gravity at the surface from a global model that carries all the requirements of dynamical consistency. There is one sizeable concern in that the resolution over the entire planet is not uniform. This is due to the Pioneer orbit, which had a high eccentricity, causing the high latitude regions of Venus to be poorly resolved.

The Magellan (MGN) spacecraft, which went into orbit about Venus in August 1990, has returned Doppler data for gravity field reduction. However, because the high gain antenna was pointed at Venus for SAR mapping, no gravity data were acquired until the antenna was pointed back to Earth. This occurred at spacecraft altitudes higher than 2500 km, greatly reducing local gravity sensitivity. MGN has an eccentricity much smaller than PVO, so there is new information in the polar regions. Present reductions include two MGN circulations (486 days), which reduce uncertainties and produce somewhat better resolution.

During March, April, and May 1992 new low-altitude data have been acquired from both PVO and MGN. PVO periapsis latitude has changed 27°, from 16°N to 11°S. These data will provide better definition in the southern hemisphere, particularly over Artemis. The MGN mission now acquires periapsis gravity data for one orbit out of eight (i.e., foregoes SAR mapping for one orbit/day). Since MGN has an X-band radio signal, the data quality is a factor of 10 better than PVO. Only a small block of MGN data was acquired before its periapsis went into occultation May 16. Solar conjunction and periapsis occultation has also occurred for PVO.

In September of 1992 MGN periapsis will exit occultation and its periapsis altitude will be lowered to approximately 170 km. Periapsis will be visible from Earth for a complete 360° longitude coverage period (243 days). This should be an excellent dataset, having low X-band data noise that in turn can be combined with the PVO dataset.

In December 1992 PVO will exit periapsis occultation and low-altitude data (~150 km) in the southern hemisphere will be acquired for about one month before PVO is lost due to the lack of fuel to maneuver to safe altitudes.

In May 1993 there remains the possibility of aerobraking MGN into a circular orbit, thus allowing global uniform resolution gravity data to be acquired. One hopes that NASA has enough foresight to keep Magellan alive so this is a reality. It is anticipated that if this is done, harmonic solutions to degree and order 60–70 (5000 parameters) will be produced. One could then compare similar features globally, resolve coronae and test many interior structure models.

References: [1] Ananda M. P. et al. (1980) *JGR, 85*, 8303–8318. [2] Williams B. G. et al. (1982) *Icarus, 56*, 578–589. [3] Mottinger N. A. et al. (1985) *Proc. LPSC 15th*, in *JGR, 90*, C739–C756. [4] Phillips R. J. et al. (1979) *Science, 205*, 93–96. [5] Sjogren W. L. et al. (1980) *JGR, 85*, 8295–8302. [6] Sjogren W. L. et al. (1983) *JGR, 88*, 1119–1128. [7] Esposito P. B. et al. (1982) *Icarus, 51*, 448–459. [8] Reasenberg R. D. et al. (1981) *JGR, 86*, 7173–7199. [9] Sjogren W. L. et al. (1984) *GRL, 11*, 489–491. [10] Nerem R. S. (1991) *Eos, 72*, 174–175. [11] McNamee J. B. et al. (1992) *JGR*, in press. [12] Konopliv A. R. (1992) private communication of results to be published (AGU presentation in Montreal, Canada).

N93-14378

DIFFERENT TYPES OF SMALL VOLCANOS ON VENUS.

E. N. Slyuta[1], I. V. Shalimov[2], and A. M. Nikishin[2], [1]Vernadsky Institute, Russian Academy of Science, 117975 Moscow, Russia, [2]Moscow University, Moscow, Russia.

One of the studies of volcanic activity on Venus is the comparison of that with the analogous volcanic activity on Earth. The preliminary report of such a comparison and description of a small